Coconut kernel-derived activated carbon as electrode material for electrical double-layer capacitors

5 authors, including:

Brij Kishore
CSIR-CMERI

53 PUBLICATIONS   851 CITATIONS

Shanmughasundaram Duraisamy
Ulster University

22 PUBLICATIONS   352 CITATIONS

Tirupathi R. Penki
Bar Ilan University

68 PUBLICATIONS   2,027 CITATIONS

Coconut kernel-derived activated carbon as electrode material for electrical double-layer capacitors

Brij Kishore · D. Shanmughasundaram ·
Tirupathi Rao Penki · N. Munichandraiah

Abstract Carbonization of milk-free coconut kernel pulp is carried out at low temperatures. The carbon samples are activated using KOH, and electrical double-layer capacitor (EDLC) properties are studied. Among the several samples prepared, activated carbon prepared at 600 °C has a large surface area (1,200 m^2 g^{-1}). There is a decrease in surface area with increasing temperature of preparation. Cyclic voltammetry and galvanostatic charge–discharge studies suggest that activated carbons derived from coconut kernel pulp are appropriate materials for EDLC studies in acidic, alkaline, and non-aqueous electrolytes. Specific capacitance of 173 F g^{-1} is obtained in 1 M H$_2$SO$_4$ electrolyte for the activated carbon prepared at 600 °C. The supercapacitor properties of activated carbon sample prepared at 600 °C are superior to the samples prepared at higher temperatures.

Keywords Coconut kernel · Activated carbon · Supercapacitor · Specific capacitance

1 Introduction

Carbon is known in a variety of forms such as charcoal, soot, coal, diamond, etc., from prehistoric times. Carbon is explored for a wide range of applications, which include metallurgy, adsorption of odorous vapors, medicine, water purification, sugar refinery, etc., since ancient times [1]. In recent years, the importance of carbon has become

B. Kishore · D. Shanmughasundaram · T. R. Penki ·
N. Munichandraiah (✉)
Department of Inorganic and Physical Chemistry, Indian
Institute of Science, Bangalore 560012, India
e-mail: muni@ipc.iisc.ernet.in

extensive in electrochemical energy storage and conversion applications [2]. Starting from the use of conductive carbons to enhance electronic conductivity of MnO$_2$ cathode mix in Leclanche cells, the development of lithium–carbon monofluoride cells, lithium-ion cells, fuel cells, and electrical double-layer capacitors (EDLCs) in recent years depends on favorable properties of carbons in electrochemical devices [3–8]. The importance of carbons in this area of application has been increasing.

At present, Li-ion batteries exist at the fore front among electrochemical energy conversion devices, as they offer a high energy density [6, 7]. Although extensive research efforts are underway to enhance the performance characteristics of Li-ion batteries, they generally suffer from low power density. Supercapacitors offer high power density but with low energy density [3, 9]. A combination of high energy battery and a high power supercapacitor in a hybrid configuration is expected to be useful for both high energy and high power applications. Among several types of supercapacitors, EDLCs are the most common devices developed at present. Carbon-based electrode materials with high surface area are used for fabrication of EDLCs. These electrodes store charge electrostatically by adsorption of ions of the electrolyte resulting in the development of double-layer capacitance. Desorption of ions from the electrode surface takes place when the electrode is discharged. The reversible adsorption–desorption processes facilitate EDLCs to have an extended charge–discharge cycle-life. Development of the appropriate carbon materials for applications in supercapacitors with high capacitance and long cycle-life is a challenging area at present.

There are several precursors, which are useful for preparation of appropriate forms of carbons for electrochemical energy storage applications. Among them, biomass sources occupy importance as bio-waste can be

converted into an economical and useful product [10]. The biomass sources investigated for preparation of carbons include bamboo [11], firwood [12, 13], coffee shell [14], corn grains [15], potato starch [16], wheat straw [17], walnut shell [18], cherry stone waste [19], pistachio shell [20, 21], sorghum pith [22], sunflower seed shells [23], apple pulp [24], waste tea leaves [25], rubber wood sawdust [26], sugar cane bagasse [27], waste paper [28, 29], hardwood tree [30], ginko shell [31], etc. Porous graphene-like nanosheets of carbons are prepared from coconut shell by simultaneous treatment with graphite catalyst ($FeCl_3$) and activating agent ($ZnCl_2$) [32]. Coconut kernel is used for extraction of milk and oil, and the remaining pulp is generally a waste. As large quantities of coconut kernel pulp are available from oil and food industries, it is an appropriate source for preparation of carbon. To the best of authors' knowledge, there are no reports on conversion of coconut kernel pulp into carbon for application in electrochemical energy storage and conversion.

The present study involves preparation of carbon samples by carbonization of fresh coconut kernel pulp at several temperatures followed by activation and characterization of them for EDLC properties. Interestingly, high specific capacitance (SC) values are measured for activated coconut kernel carbon in acidic and alkaline media as well as in a non-aqueous electrolyte.

2 Experimental

Kernel from well-ripened coconuts was grated, and milk was extracted by grinding repeatedly in warm water using a kitchen grinding machine and squeezing using a cloth. The pulp was washed with double distilled water under stirring several times, finally rinsed with a mixture of double distilled water and acetone (1:1 by volume) and dried at 120 °C for 12 h, followed by heating at 300 °C for 3 h. Large quantities of volatile parts are removed during this process. The precursor samples were carbonized at 600, 800, and 1,000 °C for 3 h in a tubular furnace under N_2 flow. The furnace was heated from room temperature to the required temperature at a rate of 10 °C min^{-1}. After carbonization, it was allowed to naturally cool to the ambient temperature under N_2 flow. The yield of carbonization was found to be in the range of 41–46 %.

The carbon samples were activated using KOH as the activating agent [33]. For this purpose, 1.2 g of KOH was dissolved in 25 ml of ethanol, 300 mg of the as-prepared carbon sample was added and stirred for 30 min. The slurry was then transferred to an alumina boat and placed in a tubular furnace. The furnace was first heated slowly to 70 °C for evaporation of the solvent under N_2 flow for about 1 h, then the temperature was raised to 700 °C,

Table 1 C, H, N analysis of the various prepared and activated carbon samples

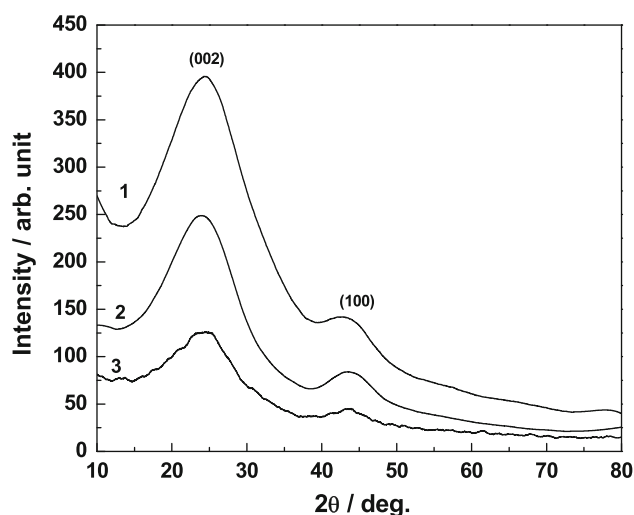| Samples	Weight percentage			
	Carbon	Hydrogen	Nitrogen	Total
Precursor	66.4	6.3	2.8	75.5
C600	82.4	2.8	3.6	88.8
C800	81.9	1.7	1.6	85.2
C1000	84.1	2.5	1.7	88.3
AC600	74.5	3.4	2.2	80.1
AC800	80.7	2.2	1.5	84.4
AC1000	75.4	1.8	1.9	79.1

Fig. 1 Powder XRD patterns of AC600 (*1*), AC800 (*2*), and AC1000 (*3*) samples

maintained for 1 h and then allowed to cool under N_2 flow. The resulting mixture was washed with 1 M HCl and then with copious amounts of double distilled water till the run off had a pH $\approx$ 7. It was finally washed with acetone and dried at 120 °C under reduced pressure for 12 h. The yield of activated carbon was in the range of 78–87 wt%. The carbon samples as prepared at 600, 800, and 1,000 °C, respectively, are referred to as C600, C800, and C1000 and the corresponding activated samples as AC600, AC800, and AC1000.

The carbon content of the samples was analyzed using a Thermo Finnigan FLASH EA 1112 CHN analyzer. The carbon samples were characterized by powder X-ray diffraction (XRD) on a Philips X'Pert Pro diffractometer at 40 kV and 30 mA using Cu Kα ($\lambda = 1.5418$ Å) as the radiation source, and the data were collected at 2θ ranging from 10 to 80° at a rate of 2° min^{-1}. Raman spectra were recorded using a Horiba Jobin–Yvon LabRam HR
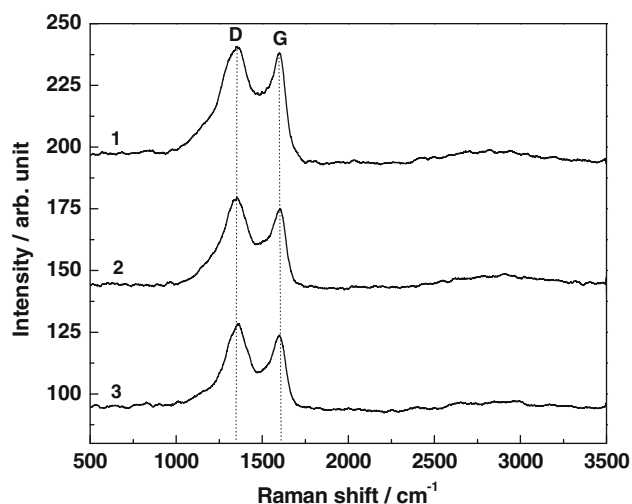
Fig. 2 Raman spectra of AC600 (*1*), AC800 (*2*), and AC1000 (*3*) samples

Table 2 I_D/I_G ratio and FWHM for all the activated carbon samples

Samples	I_D/I_G	FWHM (cm^{-1})	
		D	G
AC600	1.01	1,169	530
AC800	1.03	897	644
AC1000	1.04	783	395

spectrometer having a laser source of wavelength 532 nm and power 0.28 mW. The morphology was examined using a FEI Co. scanning electron microscope (SEM) model Sirion. Nitrogen adsorption–desorption isotherms were recorded at −196 °C using Micromeritics surface area analyzer model ASAP-2020. The specific surface area was calculated by the Brunauer–Emmett–Teller (BET) method from the adsorption branch. The pore size distribution was calculated by Barrett–Joyner–Halenda (BJH) method from desorption branch of the isotherm.

For fabrication of electrodes, active material (85 wt%), Ketjen black of surface area 1,400 m^2 g^{-1} (15 wt%), and polyvinylidine fluoride (5 wt%) were mixed in a mortar and a few drops of *n*-methyl pyrrolidone were added to obtain a slurry. The slurry was applied on pre-treated stainless steel (SS) foil (grade 304) of area 0.58 cm^2 for studies in aqueous media or on a circular pre-treated SS disk of 12 mm diameter for studies in non-aqueous medium and dried at 100 °C. Coating and drying steps were repeated so as to get a loading level of the active material weight in the range 0.5–1.0 mg cm^{-2}. Finally, the electrodes were dried at 100 °C under reduced pressure for 12 h. Average coating thickness was 1.5 μm. The SS substrate (thickness 0.2 mm) was polished by successive grades of emery, washed thoroughly, etched in dilute HNO$_3$, washed again with double distilled water, rinsed with acetone, and air dried before using as the substrate. Cyclic voltammetry of SS substrate in 1 M H$_2$SO$_4$ provided negligibly small current without any current peaks in the potential range used in the present study, thus ensuring electrochemical stability of the current collector. Saturated calomel electrode (SCE) was used as the reference electrode and Pt-foil (area ~5 cm^2) as the counter electrode

for studies in aqueous electrolytes in a glass cell. Potential values reported are against SCE reference. For studies in non-aqueous medium, a home-made Swagelok-type cell assembly was used in a symmetrical configuration with two identical electrodes separated by an absorbent glass matrix separator soaked in the electrolyte. The electrolytes used were 1 M H$_2$SO$_4$ and 1 M KOH for aqueous studies and 1 M tetraethylammonium tetrafluoroborate (TEABF$_4$) in propylene carbonate (PC) for non-aqueous studies. Swagelok cells were assembled in argon filled MBraun glove box model UNIlab. Cyclic voltammetry and charge–discharge cycling experiments were carried out using a bio-logic multi-channel potentiostat/galvanostat model VMP3. All experiments were carried out at 22 ± 2 °C.

3 Results and discussion

3.1 Preparation of carbons

Generally, carbons are prepared by pyrolysis of carbonaceous materials of vegetable origin such as wood, nutshells, etc., or polymers such as polyacrylonitrile, phenolics, etc. The carbonaceous precursors need to contain high carbon content and low inorganic (ash) materials [33]. The results of chemical analysis of the coconut kernel precursor as well as the as-prepared and the activated carbon samples are listed in Table 1. The carbon content present in the coconut kernel pulp precursor is 66.4 wt%. Hydrogen (6.3 wt%) and nitrogen (2.8 wt%) are also present in small quantities. The presence of hydrogen is due to the moisture still contained in the coconut kernel pulp after drying. A comparison of carbon content of several precursors is made by Manocha [34]. The carbon content varies in a wide range from 40 to 45 wt% for soft wood, 40 to 42 wt% for hard wood, 35 to 40 wt% for lignin, 40 to 45 wt% for nutshells, etc., among vegetable sources. Carbon contents of 65–80 wt% for soft coal, 70–85 wt% for petroleum coke, 85–95 wt% for hard coal, etc., are reported [34]. When compared with the carbon content generally present in the vegetable sources (40–45 wt%), coconut kernel pulp has high (66.4 wt%) carbon. Furthermore, the yield of carbon from the precursor is 41–46 wt% (cf. Sect. 2). High carbon content as well as an attractive yield indicates that the

**Fig. 3** SEM images of **a** C600, **b** C800, and **c** C1000 samples
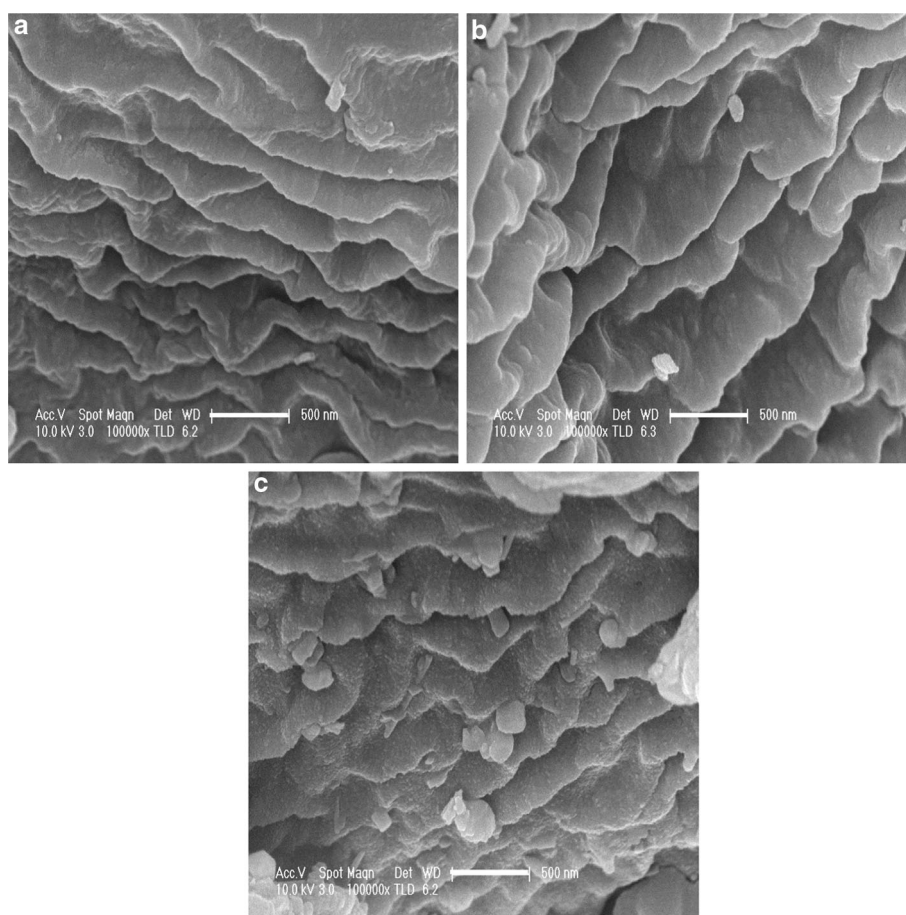
coconut kernel is suitable for preparation of carbons. Subsequent to the carbonization at different temperatures as well as the activation, the carbon content increases and the hydrogen content decreases (Table 1). The carbon content in C600, C800, and C1000 samples is in the range of 82–84 wt%, and the hydrogen content is in the range of 1.7–2.8 wt%. Thus, there is considerable increase in carbon and a decrease in hydrogen subsequent to carbonization of the coconut kernel pulp. There is a marginal decrease in the carbon content (74–81 wt%) in the activated samples in comparison with the as-prepared samples (Table 1). The ash content obtained by burning the activated carbon samples at 800 °C in air was in the range of 2–4 wt%.

3.2 Physicochemical studies

Powder XRD patterns of the as-prepared and activated carbon samples were recorded. The patterns of activated samples are shown in Fig. 1. The patterns of the as-prepared samples (not shown) are similar to the patterns shown in Fig. 1. The XRD patterns mainly consist of two broad reflections at 24.2 and 43.5° corresponding to (002) and (100) planes of hexagonal close packing of small

crystallites. The value of d-spacing is about 3.65 Å, which is greater than 3.35 Å expected for graphite. This is due to disorder nature of the carbon samples. Also, the activation procedure leads to expansion of graphitic (G) layers. It is known that carbons prepared at low temperature range (500–1,200 °C) exhibit XRD patterns with broad reflections corresponding to (002), (100), and (110) planes of graphite with decreasing intensity [35]. The origin of broad reflection of (002) plane is attributed to a small number of well-stacked layers with a uniform inter-layer distance greater than that of graphite (3.35 Å). The XRD patterns (Fig. 1) are similar to the patterns reported by Dahn et al. [35]. For cokes and soft carbons, only (002) and (004) reflections due to stacking of the layers are observed. The (100) and (110) reflections are due to the inplane order [36]. The inter-layer spacing values ranging from 3.77 to 4.10 Å are reported for various samples of carbon prepared from rice husk [37] and potato starch [38]. Factors which affect the positions and width of diffraction peaks include finite crystal size broadening, fluctuation in lattice parameters, and strains [35]. Antonio et al. [39] reported XRD results of different carbon nanospheres with d-spacing ranging from 3.2 to 3.9 Å. The values of d-spacing of

Fig. 4 SEM images of **a** AC600, **b** AC800, and **c** AC1000 samples
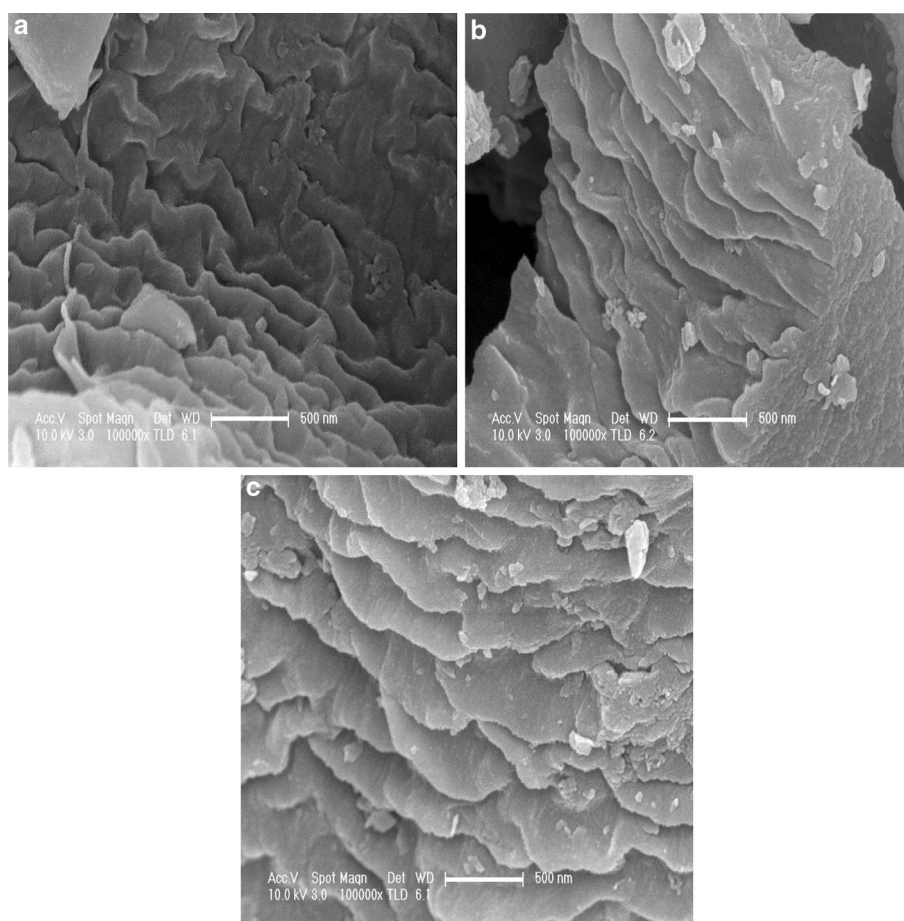
activated carbons prepared from coconut kernel pulp in the present study agree with the values reported [39].

Raman spectra of the activated samples are presented in Fig. 2. There are two bands at 1,350 and 1,599 cm^{-1} corresponding to disordered (D) and graphitic (G) planes for all the three samples. Tuinstra and Koenig [40] reported Raman spectra of several G materials. Single crystals of graphite exhibited only a single band at 1,575 cm^{-1}, whereas the other G samples exhibited an additional band near 1,355 cm^{-1}. The intensity of 1,355 cm^{-1} band increased with an increase in the amount of unorganized carbon in the sample and also to a decrease in the crystal size. This band was attributed to Raman active modes of A_{1g} type [40–43]. The Raman band at 1,575 cm^{-1} was present for all graphite samples studied [40–43]. A positive shift in frequency (~ 15 cm^{-1}) was observed in some samples with small crystal sizes. This band was attributed to E_{2g} mode of vibrations, which was restricted to the motion of atoms to the plane of the carbon atoms [40–43]. Raman spectra (Fig. 2) of AC600, AC800, and AC1000 samples agree with spectra reported in [40, 41] for D carbon materials. The ratios of intensities of D and G bands (I_D/I_G) as well as full width at half maxima (FWHM) are

listed in Table 2. SEM images (Figs. 3, 4) indicate that both as-prepared carbons and activated carbons have micro-sheet-like morphology. This type of morphology is expected as the coconut kernel pulp precursor is fibrous in nature.

N_2 adsorption–desorption isotherms and the corresponding BJH curves of AC600, AC800, and AC1000 samples are presented in Fig. 5. The isotherm of AC600 sample resembles Type I isotherm with a rapid increase in volume of adsorbed N_2 at the initial stages of increase in relative pressure. The quantity of N_2 reaches a limiting value of about 380 cm^3 g^{-1} at P/P_o of 0.3. This type of isotherm is typical for microporous solids having relatively small external surfaces [44]. Accordingly, the BJH curve (Fig. 5a, inset) indicates the presence of micropores of less than 2 nm diameter. On the other hand, AC800 and AC1000 samples exhibit Type IV isotherm (Fig. 5a, b). The adsorption–desorption isotherms are separated by a hysteresis loop, which is associated with capillary condensation taking place in mesopores. The corresponding BJH curves indicate the presence of pores greater than 2 nm diameter. Thus, AC600 sample is populated significantly with micropores, whereas AC800 and AC1000 are
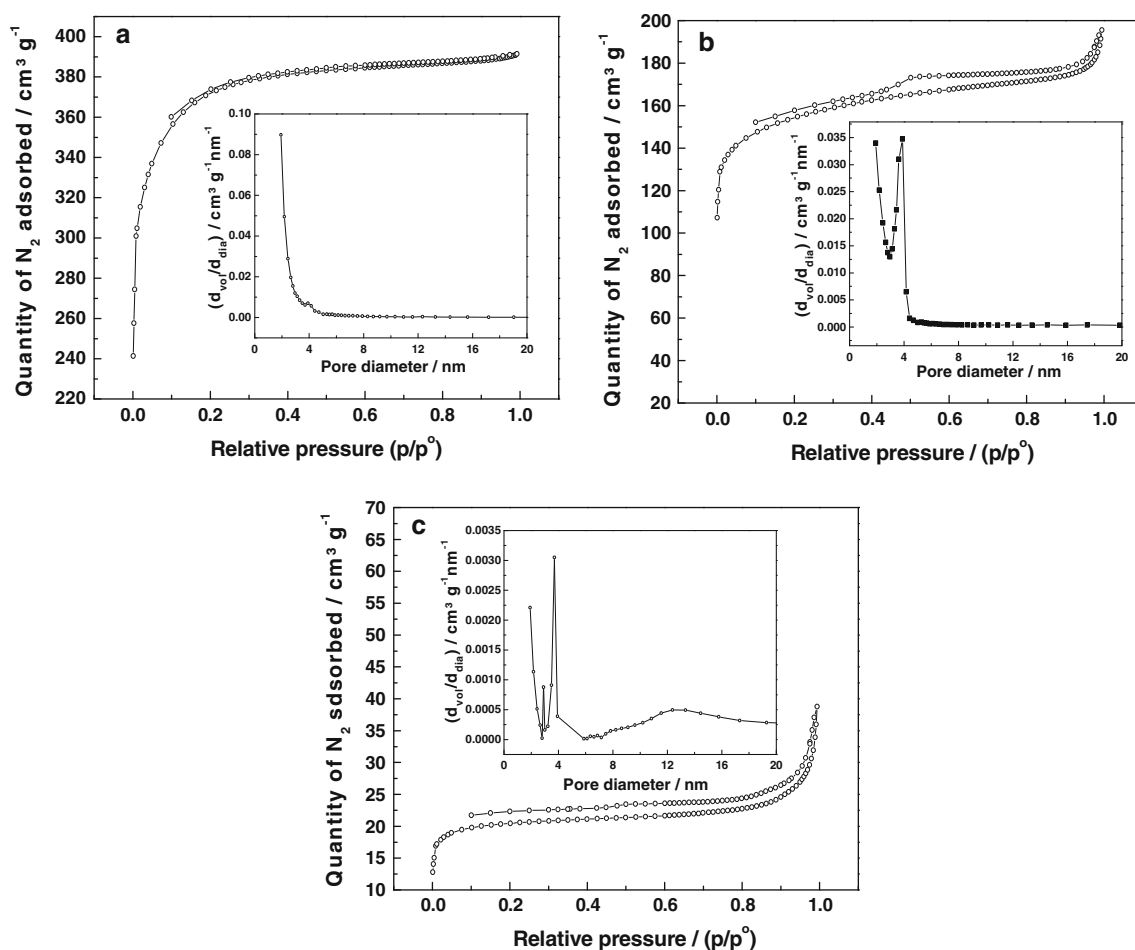
Fig. 5 Nitrogen adsorption–desorption isotherms of **a** AC600, **b** AC800, and **c** AC1000 samples and the corresponding BJH pore distribution curves in *insets*

Table 3 Specific surface area, total pore volume, micropore surface area, and micropore volume and DFT pore volume of the various prepared and activated carbon samples

Samples	Specific surface area ($m^2 g^{-1}$)	Total pore volume ($cm^3 g^{-1}$)	Micropore surface area ($m^2 g^{-1}$)	Micropore volume ($cm^3 g^{-1}$)	DFT pore volume ($cm^3 g^{-1}$)
C600	278	0.142	262	0.127	0.087
C800	129	0.085	89	0.043	0.017
C1000	5	0.016	9	0.004	0.001
AC600	1,200	0.605	934	0.457	0.267
AC800	502	0.302	363	0.178	0.157
AC1000	66	0.060	53	0.026	0.011

rich with mesopores. It was reported that micropores are more important than mesopores for facilitating high SC of carbon materials [45]. It was shown that there was a significant increase in SC of carbide-derived carbon by decreasing the average pore size from 1.5 nm to about 0.7 nm [45]. Analysis of adsorption isotherm by density field theory (DFT) provides characteristics of micropores [46]. The surface area and pore properties are listed in Table 3. It is interesting to notice that the surface area of

AC600 sample is as high as 1,200 $m^2 g^{-1}$. The area values of AC800 and AC1000 samples are 502 and 66 $m^2 g^{-1}$, respectively. The effect of activation of carbon samples is also inferred from Table 3. The samples possess less surface area before activation, and it increases by several times after activation. The carbonization temperature influences significantly on surface area and porosity. The value of 1,200 $m^2 g^{-1}$ measured for AC600 samples is very attractive for supercapacitor studies, as detailed in the
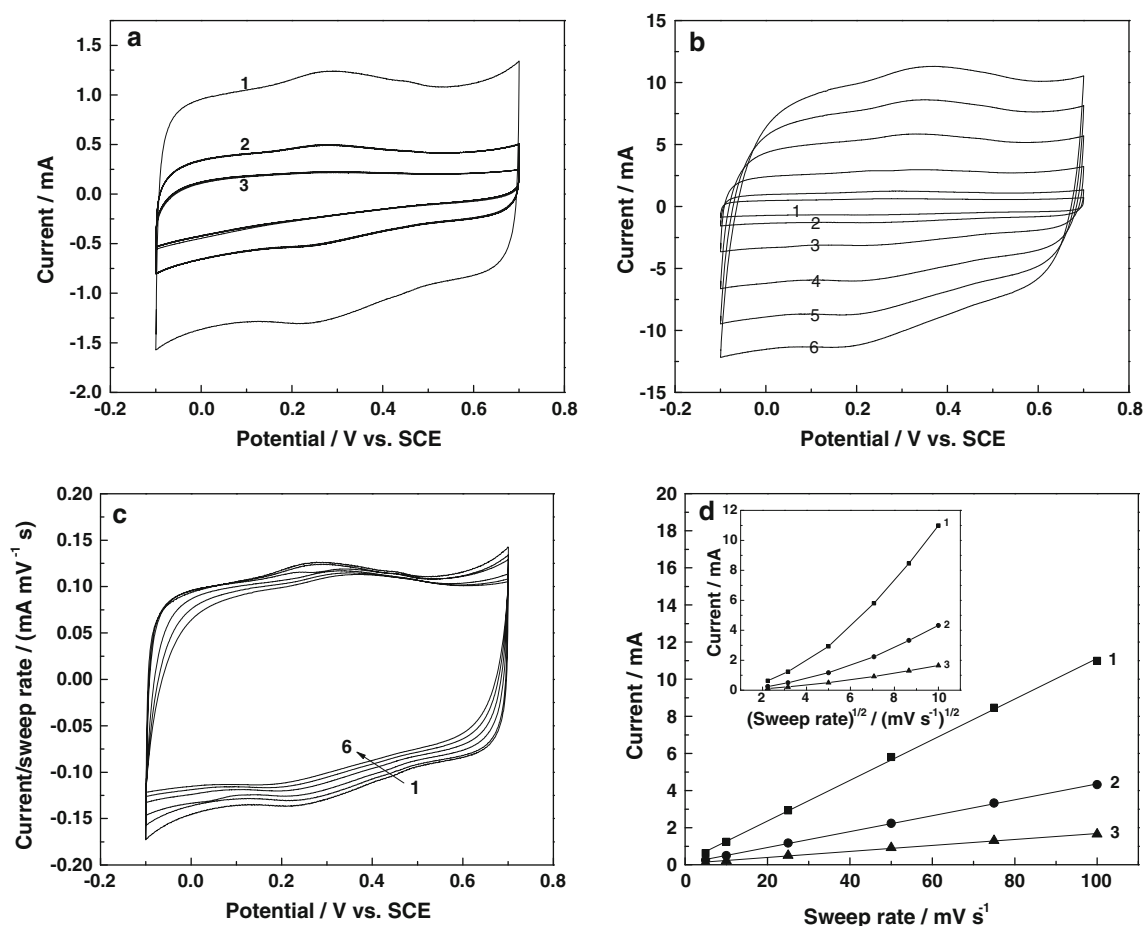
Fig. 6 In 1 M H_2SO_4, **a** cyclic voltammograms of AC600 (*1*), AC800 (*2*), and AC1000 (*3*) samples at 10 mV s^{-1}, **b** voltammograms of AC600 sample at sweep rates 5 (*1*), 10 (*2*), 25 (*3*), 50 (*4*), 75 (*5*), and 100 (*6*) mV s^{-1}, **c** current/sweep rate versus potential for AC600 sample and **d** current versus sweep rate for AC600 (*1*), AC800 (*2*), and AC1000 (*3*) samples and the *inset* same as **d** but with square root of sweep rate

following sections. Additionally, the DFT micropore volume (Table 3) is also the highest for AC600 sample.

3.3 Electrochemical studies in 1 M H_2SO_4

As the activated carbon samples have greater surface area and pore properties than the as-prepared samples (Table 3), electrochemical studies were performed with the activated samples only. The activated carbon samples were subjected to cyclic voltammetry in 1 M H_2SO_4 at several potential ranges. It was found that the voltammograms were rectangular in the potential range between −0.10 and 0.70 V. Cyclic voltammograms of AC600, AC800, and AC1000 samples recorded at 10 mV s^{-1} sweep rate are shown in Fig. 6a for comparison. The shape of voltammograms is rectangular for all samples. However, current value at any potential is the highest for AC600 sample and it is the least for AC1000 sample. This indicates that AC600 sample has better supercapacitor properties than the other two samples.

The electrodes were subjected to cyclic voltammetry at several sweep rates, and the data of AC600 sample are shown in Fig. 6b. Similar voltammograms were recorded for AC800 and AC1000 samples also. Cyclic voltammetric currents are normalized with respect to sweep rate and replotted in Fig. 6c as current/sweep rate versus potential. All voltammograms nearly merge indicating EDLC property of the carbon sample. This is further illustrated by plotting the anodic current measured at 0.30 V against sweep rate (Fig. 6d) as well as against square root of sweep rate (Fig. 6d, inset). Current increases linearly with sweep rate (Fig. 6d) for all activated carbon samples, whereas the plots of current versus square root of sweep rate are non-linear (Fig. 6d, inset). These data suggest that the measured current is due to charging of double-layer and diffusion-limited electrochemical reactions are absent. Thus the activated coconut kernel carbon samples are suitable for supercapacitor studies. The electrodes were subjected to charge–discharge cycling between −0.10 and 0.70 V in
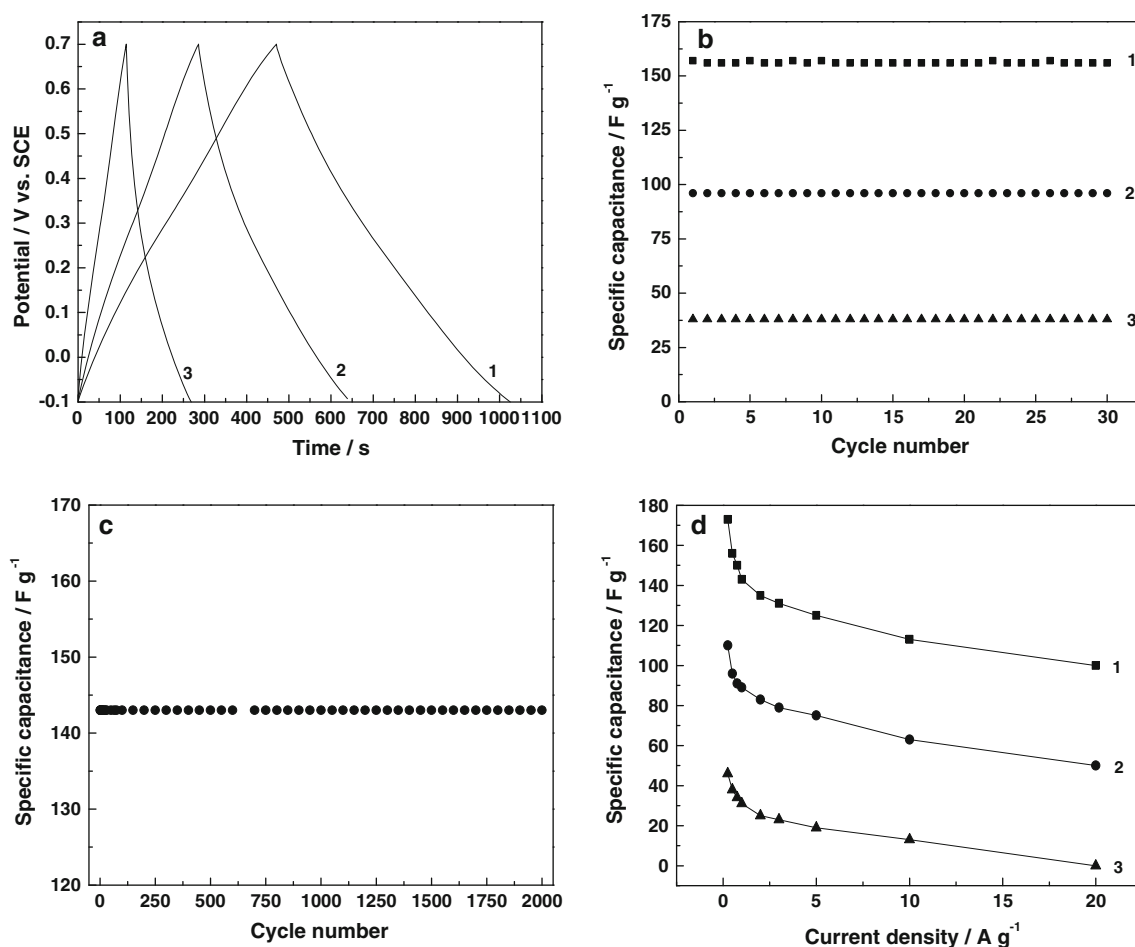
Fig. 7 In 1 M H$_2$SO$_4$, **a** charge–discharge curves at 0.25 A g^{-1} for AC600 (*1*), AC800 (*2*), and AC1000 (*3*) samples, **b** cycle-life data for AC600 (*1*), AC800 (*2*), and AC1000 (*3*) samples at 0.50 A g^{-1}, **c** cycle-life data for AC600 sample at 1.00 A g^{-1} and **d** specific capacitance versus current density for AC600 (*1*), AC800 (*2*), and AC1000 (*3*) samples

1 M H$_2$SO$_4$ at different current densities. The variations of potential with time during charge and discharge processes are shown in Fig. 7a for AC600, AC800, and AC1000 carbon samples, typically, at a current density of 0.20 mA cm^{-2} (0.25 A g^{-1}). The plots are linear, which is a characteristic feature of a capacitor material. The time required for completing one charge–discharge cycle is the highest for AC600 sample and it is the least for AC1000 sample, thus, suggesting that the highest capacitance is obtained from AC600 sample. The specific discharge capacitance (SC) values are calculated from the galvanostatic current (I), time of discharge (t), and mass of activated carbon (m) using the following equation:

$$SC = It/(m\Delta E), \tag{1}$$

where ΔE is the potential range. The values of SC calculated from Fig. 7a for AC600, AC800, and AC1000 samples, respectively, are 173, 110, and 46 F g^{-1} at 0.20 mA cm^{-2} (0.25 A g^{-1}). Charge–discharge cycling was repeated over

30 cycles for the three activated carbon electrodes at 0.40 mA cm^{-2} (0.50 A g^{-1}), and the data are presented in Fig. 7b. Discharge SC is stable and consistent throughout the cycle-life test. An electrode made of AC600 was subjected to an extended charge–discharge cycling (2,000 cycles) at a current density of 0.82 mA cm^{-2} (1.00 A g^{-1}) as shown in Fig. 7c. Constant SC of 130 F g^{-1} is obtained throughout the extended cycling study. The activated carbon electrodes were cycled with different current densities, and the variation of discharge SC is shown in Fig. 7d. There is a decrease in SC with current density, as expected, for all electrodes. It is interesting to notice that SC obtained from AC600 sample is about 100 F g^{-1} at a specific current as high as 16.4 mA cm^{-2} (20 A g^{-1}). However, very low values of SC are obtained for AC800 and AC1000 samples at 16.4 mA cm^{-2} (20 A g^{-1}).

For the purpose of comparison of SC obtained in the present study with literature values, a few important results are listed in Table 4. The reported SC values in H$_2$SO$_4$

Table 4 Comparison of specific capacitance values from literature

S. Nos.	Electrolytes	Materials	BET surface area ($m^2\ g^{-1}$)	Specific capacitance ($F\ g^{-1}$)	Measured at	References
1	H_2SO_4	Pistachio shells	1,009–1,096	60–125	$10\ mV\ s^{-1}$	[20]
			1,013–2,145	83–122	$25\ mV\ s^{-1}$	[21]
		Firwood	1,016	96	$25\ mV\ s^{-1}$	[12]
			2,821	197	$3\ mA\ cm^{-2}$	[13]
		Rubberwood sawdust	683	33	$1\ mV\ s^{-1}$	[26]
		Sorghum pith	17–35	320	$10\ mV\ s^{-1}$	[22]
		Sugar cane bagasse	1,788	300	$0.25\ A\ g^{-1}$	[27]
		Apple pulp	589–1,093	109–187	–	[24]
		Cherry stones	954–1,292	174–232	–	
		Cherry stone waste	1,100–1,300	230	–	[19]
2	KOH	Walnut shell	1,197	292	–	[18]
		Ginko shell	1,775	178	$500\ mV\ s^{-1}$	[31]
		Sunflower seed shell	1,371–2,821	311	$0.25\ A\ g^{-1}$	[23]
		Waste tea leaves	2,245–2,841	275–330	$1\ A\ g^{-1}$	[25]
		Coconut shell	1,874	276	$1\ A\ g^{-1}$	[32]
		Coffee shells	842	150	$1\ mV\ s^{-1}$	[14]
		Corn grains	2,936–3,420	257	$1\ mA\ cm^{-2}$	[15]
		Recycled waste paper	416	180	$2\ mV\ s^{-1}$	[28]
		Waste paper	463	232	$5\ mA\ cm^{-2}$	[29]
		Potato starch	2,342	335	$50\ mA\ g^{-1}$	[16]
3	$MeEt_3NBF_4$	Cherry stone waste	1,100–1,300	120	–	[19]
		Wheat straw	2,316	251	$2\ mV\ s^{-1}$	[17]
4	$TEABF_4$	Bamboo	445–1,025	5–60	$1\ mV\ s^{-1}$	[11]
		Cherry stones	954–1,292	69–120	–	[24]
		Apple pulp	589–1,093	69–120	–	
		Coconut shell	1,874	196	$1\ A\ g^{-1}$	[32]
		Petroleum	400–2,900	14–44	–	[47]
		Anthracite	943–2,479	57–167	$40\ mA\ g^{-1}$	[48]
		Hardwood tree	1,909	41.4	$10\ mA\ g^{-1}$	[30]
		PVDC	2,675	155	$50\ mA\ g^{-1}$	[49]
5	KOH	Coconut kernel	1,200	173	$0.25\ A\ g^{-1}$	Present work
	H_2SO_4			173		
	$TEABF_4$			56		

medium include 197 F g^{-1} at 3 mA cm^{-2} current density for carbon prepared from fir wood [13], 300 F g^{-1} at 0.25 A g^{-1} for carbon prepared from sugar cane bagasse [27], 109–187 F g^{-1} for apple pulp [24], etc. In comparison with the reported SC values, 173 F g^{-1} obtained in the present study for high surface area, microporous, coconut kernel pulp carbon prepared at 600 °C, and activated (AC600 sample) is also a high value.

Electrostatic adsorption of ions from the electrolyte on the carbon surface during charging of the electrode occurs resulting in the formation of a double-layer capacitor. As the magnitude of capacitance is proportional to the quantity of charge, higher is the specific surface area of the carbon,

greater would be the quantity of specific ionic charge accumulating at the carbon/solution interface. As described above, the carbonization temperature has significant influence on surface area, and hence on SC of activated coconut kernel pulp carbons (AC600, AC800 and AC1000 samples). AC600 sample has a high surface area (1,200 $m^2\ g^{-1}$) and provides a high SC (173 F g^{-1}).

3.4 Electrochemical studies in 1 M KOH

The activated carbon samples were subjected to cyclic voltammetry in 1 M KOH at several potential ranges. It was found that the voltammograms were nearly rectangular in
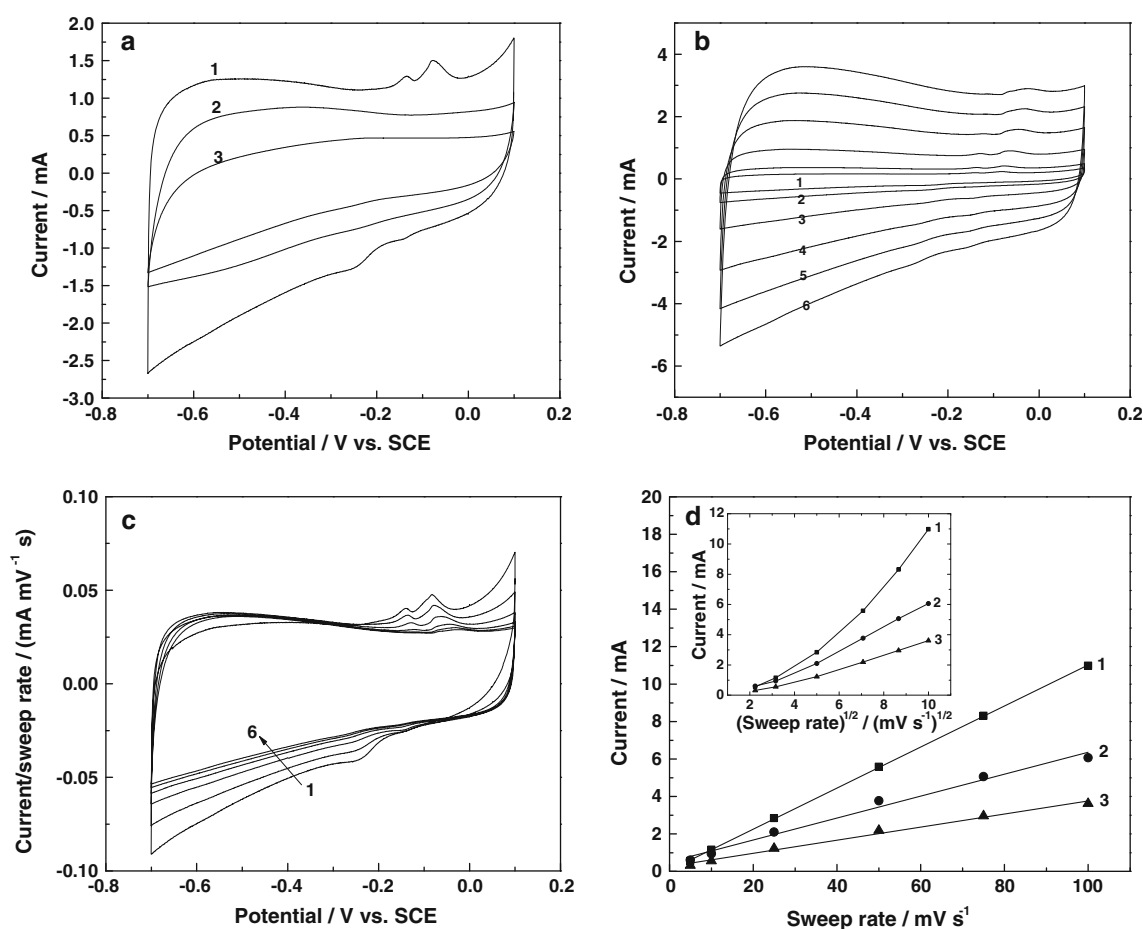
Fig. 8 In 1 M KOH, **a** cyclic voltammograms of AC600 (*1*), AC800 (*2*), and AC1000 (*3*) samples at 10 mV s^{-1}, **b** voltammograms of AC600 sample at sweep rates 5 (*1*), 10 (*2*), 25 (*3*), 50 (*4*), 75 (*5*), and 100 (*6*) mV s^{-1}, **c** current/sweep rate versus potential for AC600 sample and **d** current versus sweep rate for AC600 (*1*), AC800 (*2*) and AC1000 (*3*) samples and the *inset* same as **d** but with square root of sweep rate

the potential range between -0.70 and 0.10 V. Cyclic voltammograms of AC600, AC800, and AC1000 recorded at 10 mV s^{-1} sweep rate are shown in Fig. 8a for comparison. The current value at any potential follows the order AC600 > AC800 > AC1000 sample. This indicates that AC600 sample has superior supercapacitor properties than the other two samples in the alkaline electrolyte also similar to the acidic electrolyte. The electrodes were subjected to cyclic voltammetry at several sweep rates, and the data of AC600 sample are shown in Fig. 8b. Similar voltammograms were recorded for AC800 and AC1000 samples also. There is an increase in size of voltammograms on increasing sweep rate. Near merging of normalized voltammograms (Fig. 8c), linear increase of anodic current at 0.1 V with an increase in sweep rate (Fig. 8d), and non-linear increase of current with square root of sweep rate (Fig. 8d, inset) suggests that the activated carbon samples are suitable for double-layer supercapacitor studies in 1 M KOH electrolyte

also. The activated carbon electrodes were subjected to charge–discharge cycling between -0.70 and 0.10 V. Plots of potential versus time during charge–discharge processes are shown in Fig. 9a for AC600, AC800, and AC1000 carbon samples, at a current density of 0.83 mA cm^{-2} (1.00 A g^{-1}). The variation of potential with time is linear. The SC values calculated using Eq. (1) are 115, 98, and 83 F g^{-1}, respectively, for AC600, AC800, and AC1000 samples at 0.83 mA cm^{-2} (1.00 A g^{-1}). Charge–discharge cycling was repeated for about 30 cycles, and the data are presented in Fig. 9b. The activated carbon electrodes are stable with constant SC over about 2,000 cycles also at 0.83 mA cm^{-2} (1.00 A g^{-1}; Fig. 9c). The AC600 sample is superior to AC800 and AC1000 samples. Charge–discharge cycling was performed at several current densities and the variation of SC with current density for the activated carbons samples is shown in Fig. 9d. There is a decrease in SC with an increase in current density, as expected. It is
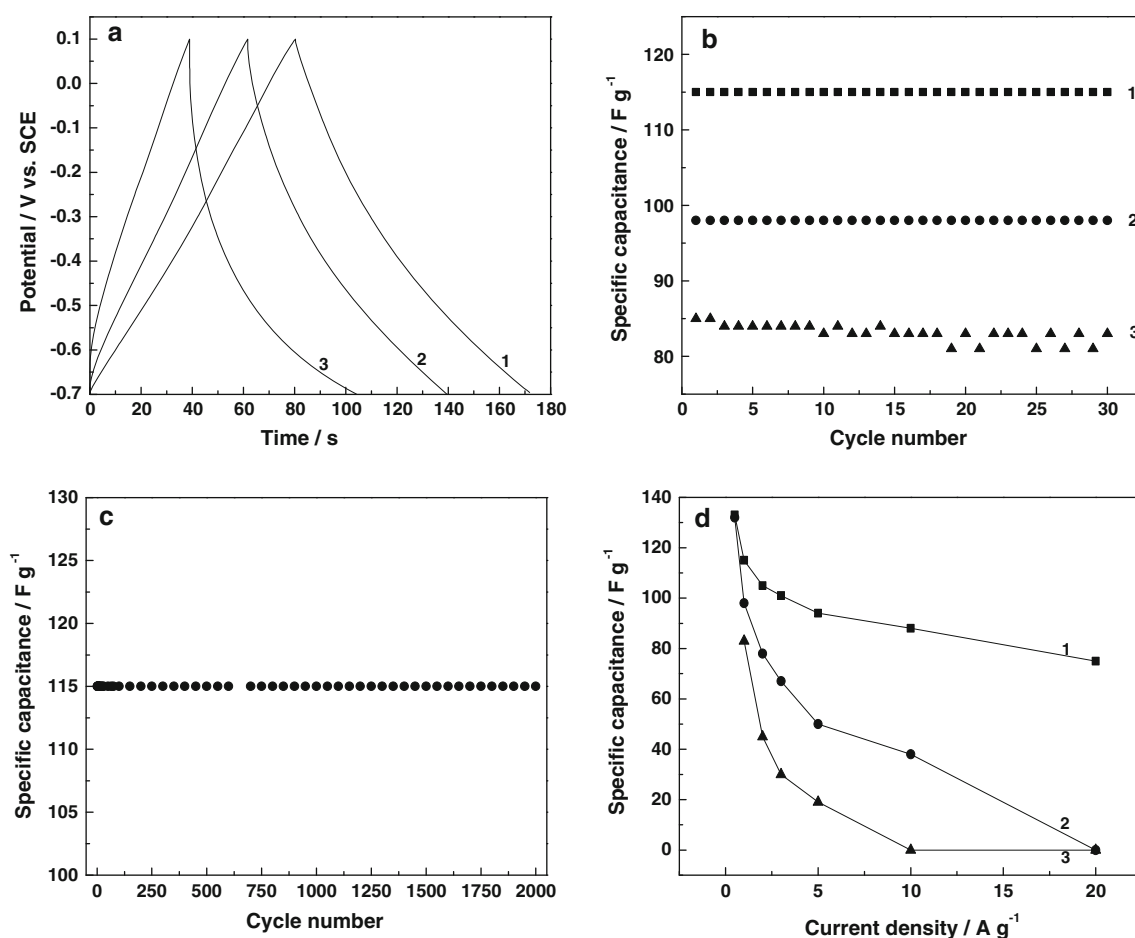
Fig. 9 In 1 M KOH, **a** charge–discharge curves at 1.00 A g^{-1} for AC600 (1), AC800 (2), and AC1000 (3) samples, **b** cycle-life data for AC600 (1), AC800 (2) and AC1000 (3) samples at 1.00 A g^{-1}, **c** cycle-life data for AC600 sample at 1.00 A g^{-1} and **d** specific capacitance versus current density for AC600 (1), AC800 (2) and AC1000 (3) samples

interesting to note that about 95 F g^{-1} is obtained at 16.6 mA cm^{-2} (20 A g^{-1}) for AC600 sample. SC values obtained for AC600 sample in 1 M KOH are comparable with literature values (Table 4).

3.5 Electrochemical studies in 1 M TEABF$_4$ in PC

Symmetrical cells consisting of AC600 activated carbon electrodes (in two electrode configuration) were subjected to cyclic voltammetry in 1 M TEABF$_4$ in PC electrolyte at several potential ranges. It was found that the voltammograms were rectangular in the voltage range between 0.00 and 3.00 V, which is greater than the voltage range in aqueous electrolytes, as expected in the non-aqueous electrolyte. Cyclic voltammogram recorded at a sweep rate of 10 mV s^{-1} is shown in Fig. 10a. The cell was subjected to cyclic voltammetry at several sweep rates, and the data

are shown in Fig. 10b. The voltammograms are broad, rectangular in shape and also the anodic and cathodic parts are nearly symmetrical. Voltammetric current increases with an increase in sweep rate (Fig. 10b). Close to merging of sweep rate-normalized voltammograms (Fig. 10c), linear increase in anodic current at 1.50 V with sweep rate (Fig. 10d) and non-linear increase in current with square root of sweep rate (Fig. 10d, inset) suggest that the activated coconut kernel carbon sample is suitable for supercapacitor studies in non-aqueous electrolyte also. The symmetrical cells were subjected to charge–discharge cycling between 0.00 and 3.00 V. Variations of voltage with time during charge–discharge processes are shown in Fig. 11a for AC600 carbon sample at various specific currents. The variation of potential with time is linear. SC of the symmetrical cell calculated using mass of carbon on both electrodes is converted into SC of a single electrode.
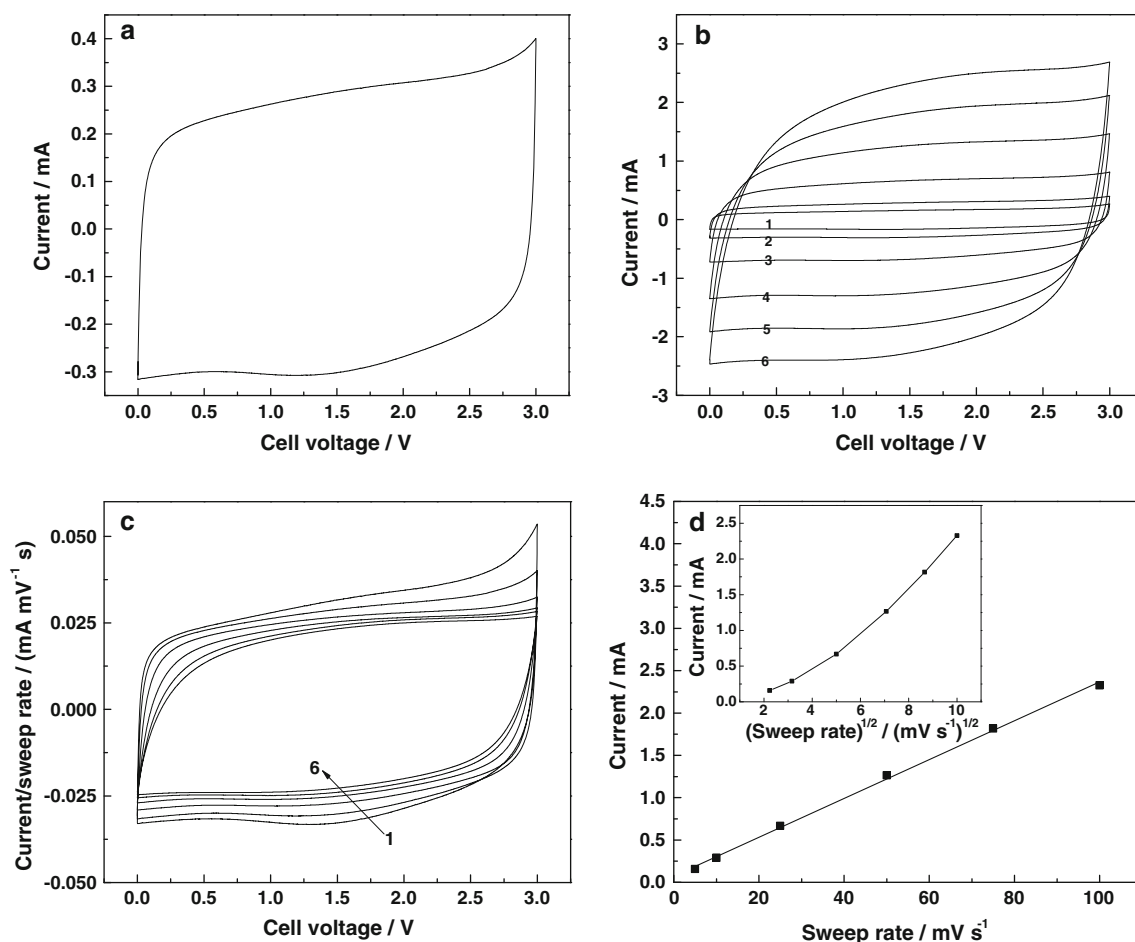
Fig. 10 In 1 M TEABF$_4$/PC, **a** cyclic voltammograms of AC600 sample at 10 mV s^{-1}, **b** voltammograms of AC600 sample at sweep rates 5 (1), 10 (2), 25 (3), 50 (4), 75 (5), and 100 (6) mV s^{-1}, **c** current/sweep rate versus potential for AC600 sample, and **d** current versus sweep rate for AC600 sample and the *inset* same as **d** but with square root of sweep rate

The SC values calculated are 56, 48, and 40 F g^{-1}, respectively, for AC600 sample at a current density of 0.25, 0.50, and 1.00 A g^{-1}. These values are comparable with the results reported in the literature (Table 4). The SC values are less in the non-aqueous electrolyte in comparison with the data in aqueous electrolytes. This is because of higher voltage, which appears in the denominator in Eq. (1) and also symmetrical cell configuration in the non-aqueous electrolyte against the three-electrode configuration in aqueous electrolytes. Charge–discharge cycling was repeated over an extended cycle-life study at a specific current of 1.0 A g^{-1}, and the data are presented in Fig. 11b. The activated carbon electrodes are stable with constant SC of 40 F g^{-1} for about 2,000 cycles. Charge–discharge cycling was performed at several current densities and the variation of SC with current density for the activated carbon sample is shown in Fig. 11c. There is a decrease in SC with increase in current density, as expected.

4 Conclusions

Milk-free coconut kernel pulp was converted into carbon samples at low temperatures. The carbon samples were activated using KOH, and EDLC properties were investigated in aqueous and non-aqueous electrolytes. Among the several samples prepared, activated carbon prepared at 600 °C had a large surface area (1,200 m^2 g^{-1}), and there was a decrease in surface area with increasing temperature of preparation. Cyclic voltammetry and galvanostatic charge–discharge studies suggested that coconut kernel pulp-derived activated carbons were appropriate for EDLC studies in acidic, alkaline, and non-aqueous electrolytes. SC of 173 F g^{-1} was obtained in 1 M H$_2$SO$_4$ electrolyte for the activated carbon prepared at 600 °C. There was a decrease in SC for low surface area samples prepared at higher temperatures. The electrochemical supercapacitor performance of activated carbon sample prepared at
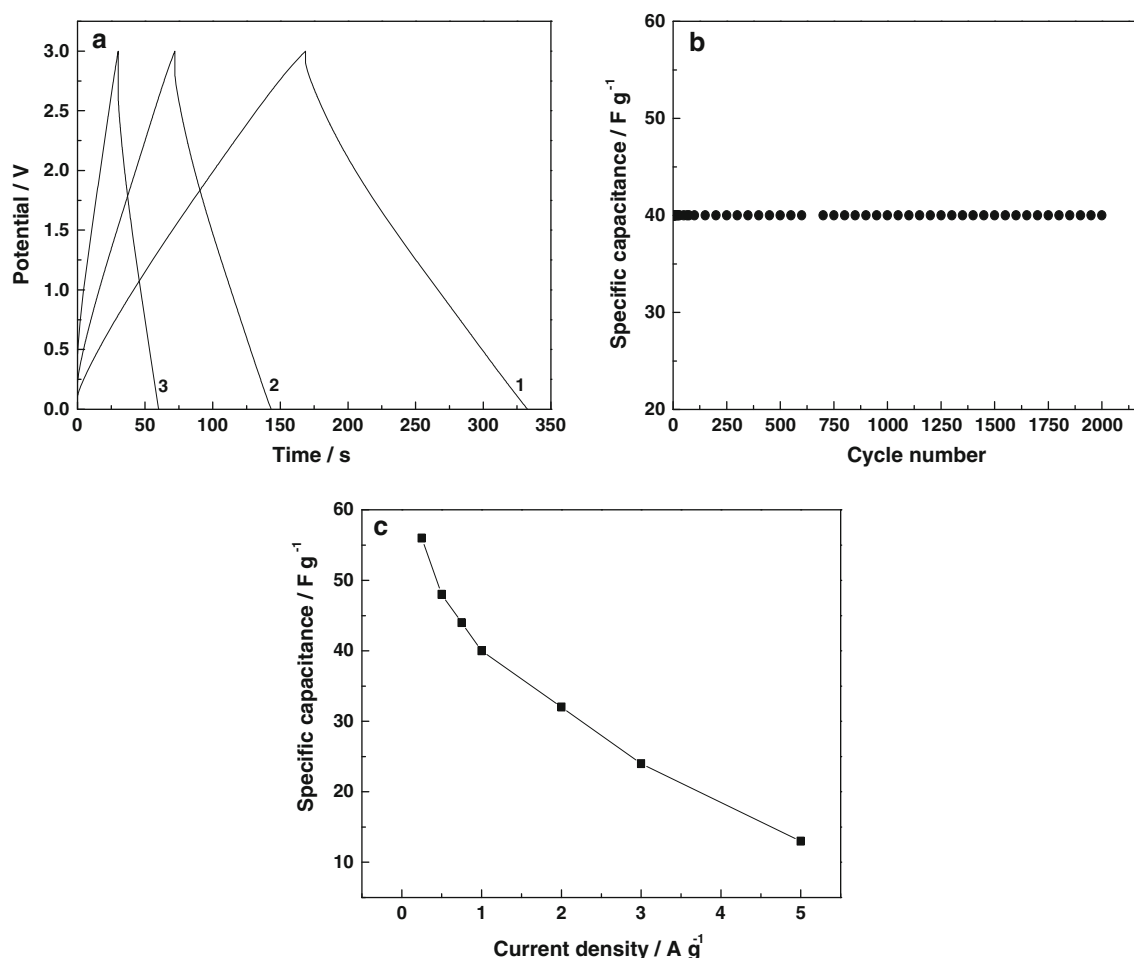
Fig. 11 In 1 M TEABF$_4$/PC, **a** charge–discharge curves at 0.25 (*1*), 0.50 (*2*), and 1.00 (*3*) A g^{-1} for AC600 sample, **b** cycle-life data for AC600 sample at 1.00 A g^{-1}, and **c** specific capacitance versus current density for AC600 sample

600 °C was superior to the samples prepared at higher temperatures.

References

1. Marsh H, Reinoso FR (2006) Activated carbon. Elsevier Science Ltd., Philadelphia, p 1
2. Winter M, Moeller KC, Besenhard JO (2004) In: Nazri GA, Pistoia G (eds) Lithium batteries: science and technology. Kluwer Academic Publishers, Boston, p 144
3. Beguin F, Frackowiak E (2013) Supercapacitors: materials, systems and applications. Wiley, Weinheim, p 1
4. Simon P, Gogotsi Y (2008) Nat Mater 7:845–854
5. Liu C, Li F, Ma LP, Cheng HM (2010) Adv Mater 22:E28–E62
6. Winter M, Brodd RJ (2004) Chem Rev 104(10):4245–4269
7. Yang Z, Zhang J, Kintner-Meyer MCW, Lu X, Choi D, Lemmon JP, Liu J (2011) Chem Rev 111:3577–3613
8. Naoi K, Ishimoto S, Miyamoto JI, Naoi W (2012) Energy Environ Sci 5:9363–9373
9. Conway BE (1999) Electrochemical supercapacitors. Kluwer Academic Publishers/Plenum Press, New York, p 1
10. Kalyani P, Anitha A (2013) Int J Hydrog Energy 38:4034–4045
11. Kim C, Lee JW, Kim JH, Yang KS (2006) Korean J Chem Eng 23(4):592–594
12. Wu FC, Tseng RL, Hu CC, Wang CC (2004) J Power Sources 138:351–359
13. Wu FC, Tseng RL, Hu CC, Wang CC (2006) J Power Sources 159:1532–1542
14. Jisha MR, Hwang YJ, Shin JS, Nahm KS, Kumar TP, Karthikeyan K, Dhanikaivelu N, Kalpana D, Renganathan NG, Stephan AM (2009) Mater Chem Phys 115:33–39
15. Balathanigaimani MS, Shim WG, Lee MJ, Kim C, Lee JW, Moon H (2008) Electrochem Commun 10:868–871
16. Zhao S, Wang CY, Chen MM, Wang J, Shi ZQ (2009) J Phys Chem Solids 70:1256–1260
17. Li X, Han C, Chen X, Shi C (2010) Microporous Mesoporous Mater 131:303–309
18. Yang J, Liu Y, Chen X, Hu Z, Zhao G (2008) Acta Phys Chim Sin 1:13–19
19. Marin MO, Fernandez JA, Lazaro MJ, Gonzalez CF, Garcia AM, Serrano VG, Stoeckli F, Centeno TA (2009) Mater Chem Phys 114:323–327
20. Wu FC, Tseng RL, Hu CC, Wang CC (2005) J Power Sources 144:302–309
21. Hu CC, Wang CC, Wu FC, Tseng RL (2007) Electrochim Acta 52:2498–2505

22. Senthilkumar ST, Senthilkumar B, Balaji S, Sanjeeviraja C, Selvan RK (2011) Mater Res Bull 46:413–419
23. Li X, Xing W, Zhuo S, Zhou J, Li F, Qiao SZ, Lu GQ (2011) Bioresour Technol 102:1118–1125
24. Centeno TA, Rubiera F, Stoeckli F (2009) 1st Spanish national conference on advances in materials recycling and eco-energy, Madrid, 12–13 November 2009
25. Peng C, Yan XB, Wang RT, Lang JW, Qu YJ, Xue QJ (2013) Electrochim Acta 87:401–408
26. Taer E, Deraman M, Talib IA, Umar AA, Qyama M, Yunus RM (2010) Curr Appl Phys 10:1071–1075
27. Rufford TE, Jurcakova DH, Khosla K, Zhu Z, Lu GQ (2010) J Power Sources 195:912–918
28. Kalpana D, Cho SH, Lee SB, Lee YS, Misra R, Renganathan NG (2009) J Power Sources 190:587–591
29. Liu MC, Kong LB, Lu C, Li XM, Luo YC, Kang L (2012) RSC Adv 2:1890–1896
30. Zhao XY, Cao JP, Morishita K, Ozaki JI, Takarada T (2010) Energy Fuels 24:1889–1893
31. Jiang L, Yan J, Hao L, Xue R, Sun G, Yi B (2013) Carbon 56:146–154
32. Sun L, Tian C, Li M, Meng X, Wang L, Wang R, Yin J, Fu H (2013) J Mater Chem A 1:6462–6470
33. Viswanathan B, Neel PI, Varadarajan TK (2009) Methods of activation and specific applications of carbon materials. Indian Institute of Technology Madras, Chennai
34. Manocha SM (2003) Sadhana 28:335–348
35. Dahn JR, Sleigh AK, Shi H, Reimers JN, Zhong Q, Way BM (1993) Electrochim Acta 38:1179–1191
36. Gong J, Wu H, Yang Q (1999) Carbon 37:1409–1416
37. Guo Y, Yang S, Yu K, Zhao J, Wang Z, Xue H (2002) Mater Chem Phys 74:320–323
38. Li W, Chen M, Wang C (2011) Mater Lett 65:3368–3370
39. Antonio NM, Romero R, Romero A, Valverde JL (2011) J Mater Chem 21:1664–1672
40. Tuinstra F, Koenig JL (1970) J Chem Phys 53:1126
41. Malard LM, Pimenta MA, Dresselhaus G, Dresselhaus MS (2009) Phys Rep 473:51–87
42. Lespade P, Jishi RA, Dresselhaus MS (1982) Carbon 20:427–431
43. Zickler GA, Smarsly B, Gierlinger N, Peterlik H, Paris O (2006) Carbon 44:3239–3246
44. Cregg SJ, Singh KSW (1982) Adsorption, surface area and porosity, 2nd edn. Academic Press, London, p 1
45. Chimola J, Yushin G, Gogotsi Y, Portet C, Simon P, Taberna PL (2006) Science 313:1760–1763
46. Jagiello J, Olivier JP (2009) J Phys Chem C 113:19382–19385
47. Qiao W, Yoon SH, Mochida I (2006) Energy Fuels 20:1680–1684
48. Zhang CX, Zhang R, Xing BL, Cheng G, Xie YB, Qiao WM, Zhan L, Liang XY, Ling LC (2010) N Carbon Mater 25(2):129–133
49. Xu B, Wu F, Mu D, Dai L, Cao G, Zhang H, Chen S, Yang Y (2010) Int J Hydrog Energy 35:632–637